Nano Research
DOI 10.1007/s12274-017-1724-y
Research Article
ISSN 1998-0124
CN 11-5974/O4

Morphology and property investigation of primary particulate matter particles from different sources

Rufan Zhang[1], Chong Liu[1], Guangmin Zhou[1], Jie Sun[1], Nian Liu[1], Po-Chun Hsu[1], Haotian Wang[1], Yongcai Qiu[1], Jie Zhao[1], Tong Wu[1], Wenting Zhao[1], and Yi Cui[1,2] (✉)

[1] *Department of Materials Science and Engineering, Stanford University, Stanford, CA 94305, USA*
[2] *Stanford Institute for Materials and Energy Sciences, SLAC National Accelerator Laboratory, 2575 Sand Hill Road, Menlo Park, CA 94025, USA*

Received: 16 May 2017
Revised: 10 June 2017
Accepted: 11 June 2017

KEYWORDS

particulate matter 2.5 ($PM_{2.5}$),
source analysis,
nanofiber,
filtration,
property,
distribution,
characterization

ABSTRACT

Particulate matter (PM) pollution has become a major environmental concern in many developing countries. PM pollution control remains a great challenge owing to the complex sources and evolution processes of PM particles. There are two categories of PM, i.e., primary and secondary PM particles, and the primary PM emissions play a key role in the formation of PM pollution. Knowledge of primary PM particle compositions, sources, and evolution processes is of great importance to the effective control of PM pollution. In order to characterize PM particles effectively, their fundamental properties including the morphology, concentration distribution, surface chemistry, and composition must be systematically investigated. In this study, we collected and analyzed six types of PM_{10} and $PM_{2.5}$ particles from different sources using an *in situ* sampling approach. The concentration distributions of PM particles were analyzed and comparative analysis of the morphologies, distributions, capture mechanisms, and compositions of PM particles was conducted using scanning electron microscopy, transmission electron microscopy, X-ray photoelectron spectroscopy, and energy-dispersive X-ray spectroscopy. We found that there were significant differences in the structures, morphologies, and capture mechanisms of $PM_{2.5}$ and PM_{10} particles. The systematic comparative investigation in this work will benefit the study of evolution processes and the effective control of PM pollution in the future.

Atmospheric particulate matter (PM) is widely known as an important source of air pollution worldwide, which has become a major environmental concern owing to the large amount of PM emissions from human activities, such as emissions from traffic, industry, and power plants [1]. PM is a complex mixture of small particles and liquid droplets suspended in air, consisting of various chemical components including

Address correspondence to yicui@stanford.edu

inorganic matter (e.g., silicates, sulfates, and nitrates) and organic matter (e.g., organic carbon, elemental carbon, etc.) [2–4]. PM particles exist in various sizes, and both PM_{10} (aerodynamic diameter shorter than 10 μm) and $PM_{2.5}$ (aerodynamic diameter shorter than 2.5 μm) particles are very harmful to the environment, climate, and human health. PM_{10} particles, also called inhalable particles, can absorb more toxic substances than coarse particles and can enter the human body via deposition in the lungs through respiration, resulting in various respiratory and cardiovascular diseases [5]. Compared to PM_{10} particles, $PM_{2.5}$ particles are even more harmful. They can not only carry various toxic compounds [2–4], but also penetrate the human bronchi and lungs and even enter the alveolar cells owing to their small size, posing a serious threat to human health [6–12]. In addition, $PM_{2.5}$ particles can remain in the atmosphere for several weeks and can be transported further by atmospheric circulation. Thus, the development of PM filtration technologies has attracted much recent attention [13–21].

PM pollution control remains a great challenge owing to the very complex sources and evolution processes of PM particles. PM particles can be divided into two categories based on their sources and evolution processes: Primary PM particles [22, 23] and secondary PM particles [24, 25]. Although secondary PM particles contribute significantly to PM pollution in many places [26], primary PM source emissions play a key role in regulating atmospheric aerosol nucleation and oxidation [27]. They also affect particle growth by condensation and the photochemical production of ozone and secondary organic aerosols [28]. Therefore, systematic investigation of primary PM particles is significant.

The characteristics of PM particles, including physical, chemical, and optical properties, are closely related to their morphologies, sizes, compositions, etc. [29]. Knowledge of PM particle compositions, sources, and evolution processes is important for reducing the harmful effects of PM particles and improving air quality. Many studies from the past few years have reported the sizes, morphologies, densities, and sources of PM_{10} [30–34] and $PM_{2.5}$ particles [35–37] and their effects on human health [38–40]. In order to characterize PM particles effectively, their fundamental properties, e.g., morphology, concentration distribution, surface chemistry, composition, etc., should be analyzed systematically. This information is essential for the assessment of the harmful effects of PM particles, but cannot be obtained through mass measurement (or bulk analysis) methods alone. The bulk analysis methods have limitations since many different particles are aggregated and only an average value is presented [37]. Therefore, it is necessary to perform *in situ* sampling of individual particles and to characterize them without changing their properties. In this study, we analyzed different types of PM_{10} and $PM_{2.5}$ particles from six different sources using *in situ* sampling methods. We collected PM particles with different sizes and conducted a comparative analysis of the morphologies, concentration distributions, and compositions of PM_{10} and $PM_{2.5}$ particles using optical microscopy (OM), scanning electron microscopy (SEM), transmission electron microscopy (TEM), X-ray photoelectron spectroscopy (XPS), and energy dispersive X-ray spectroscopy (EDX). In addition, the capture mechanisms of PM_{10} and $PM_{2.5}$ particles on nanofibers were also investigated.

In situ sampling of primary PM particles is critical for the study of the original morphologies, structures, size distributions, and compositions of individual primary aerosols. A common source of primary PM particles is PM from combustion smoke of biomass, coal, plants, etc. Anthropogenic and biomass burning sources account for more than 60% of primary carbonaceous aerosol emissions, and much of the organic matter in these aerosols is concentrated potentially at or near the particle surface [37]. In the smoke from combustion, there is a large amount of PM particles of various sizes. Thus, smoke PM particles are one of the subjects of this study. In this study, six different types of PM sources were selected, namely barbecue smoke, cigarette smoke, incense smoke, wood smoke, car exhaust, and soil dust. These PM particles were captured from their sources *in situ* by ultrathin polyimide (PI) nanofibers with diameters of 200–300 nm that were fabricated through electrospinning [14, 17]. The PI nanofibers exhibited excellent PM capture capability and high thermal stability in ambient conditions (Fig. S1 in the Electronic Supplementary Material

(ESM)) [14]. In order to keep the original sizes, morphologies, and concentration distributions of the PM particles, the PM capture process was conducted for a very short time, only 5–15 s, which is much shorter than the reported sampling times, which range from several minutes to several months. Thus, the agglomeration and coalescence of tiny PM particles into larger ones can be significantly reduced, which is favorable for investigating the original properties of primary PM particles. After capturing PM particles, the PI filters were examined directly using OM, SEM, EDX, and XPS. For TEM, Lacey carbon TEM grids, which contain numerous carbon nanofibers with diameters of 10–200 nm, were used to collect the PM particles *in situ* (see Fig. S2 in the ESM). A PM counter was used to obtain the concentration distributions of the PM particles.

The overall morphologies and concentration distributions of the captured PM particles on the PI nanofibers are shown in Fig. 1 and Figs. S3–S8 in the ESM. The six different types of PM particles had different characteristics. Most of the PM particles from smoke (> 80%), i.e., barbecue smoke (Fig. 1(a) and Fig. S3 in the ESM), cigarette smoke (Fig. 1(b) and Fig. S4 in the ESM), incense smoke (Fig. 1(c) and Fig. S5 in the ESM), and wood smoke (Fig. 1(d) and Fig. S6 in the ESM),

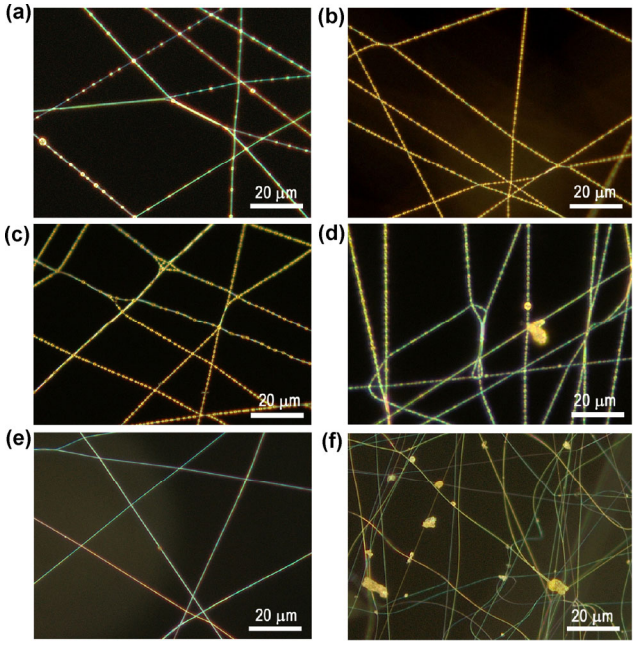

Figure 1 Overview of the PM particles from (a) barbecue smoke, (b) cigarette smoke, (c) incense smoke, (d) wood smoke, (e) car exhaust, and (f) soil dust captured on PI nanofibers.

are tiny particles with diameters shorter than 0.5 μm, and a small portion (10%–15%) of them had diameters of 1–2.5 μm. Only very few particles (< 5%) with diameters longer than 2.5 μm were found on the nanofibers, indicating that most of the PM particles (> 95%) from smoke were $PM_{2.5}$ particles. The size distribution of these $PM_{2.5}$ particles was narrow, indicating that they are uniformly dispersed in the smoke sources. As shown in Fig. 1(e) and Fig. S7 in the ESM, very few PM particles were captured from car exhaust within such a short time. The proportion of larger PM particles (with diameters longer than 2.5 μm) in soil dust was much higher than those in the other sources (Fig. 1(f) and Fig. S8 in the ESM).

The concentration distribution shows the concentrations of particles in different size ranges. A PM particle counter was used to determine the concentration distributions of PM particles from the different sources. As shown in Fig. 2(a), for almost all types of PM particles, the PM concentrations at certain sizes decreased continuously as the size increased. As shown in Fig. 1 and Figs. S3–S8 in the ESM, the PM distributions from different sources are distinctly different, and this is clearly shown in Fig. 2. For example, the total PM concentration in car exhaust was 1–2 orders lower than those in barbecue and cigarette smoke. Regarding the particles from smoke, the concentration of larger particles (diameter > 2.5 μm) in wood smoke was much higher than those in the other types of smoke because of the incomplete combustion of wood in ambient conditions (Fig. 2(a)). The PM size distribution of soil dust was more uniform than those of the other kinds of PM (Fig. 2(b)). In particular, the concentration and proportion of larger particles (diameter > 2.5 μm) in soil dust were much higher than those in other sources. In addition, the concentration of tiny PM particles (diameter < 2.5 μm), regardless of the PM type and source, was much higher than that of larger PM particles (diameter > 2.5 μm). For example, the concentration of particles with a diameter of 0.3 μm was three orders higher than that of particles with a diameter of 10 μm in incense smoke. The concentration distributions of the PM particles indicate that approximately 90% of them are smaller than 1.0 μm and can deposit directly into human alveoli. As shown in Fig. 2(b), the proportion of particles with a diameter

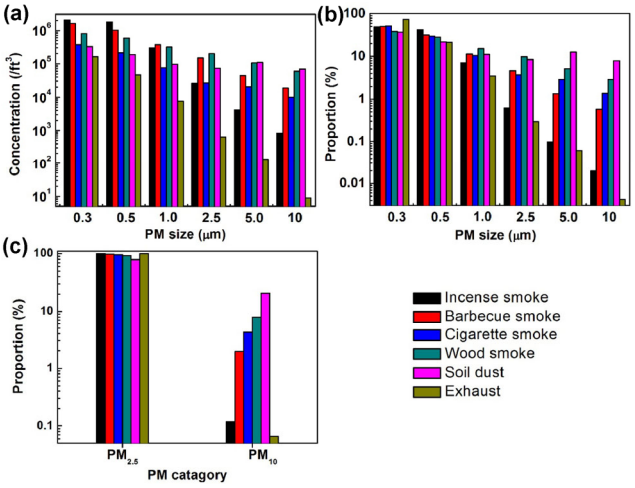

Figure 2 Concentration distributions of PM particles from different sources. (a) Concentrations of PM particles with different sizes. (b) Proportions of PM particles with different sizes. (c) Comparison of $PM_{2.5}$ and PM_{10} particles from different sources.

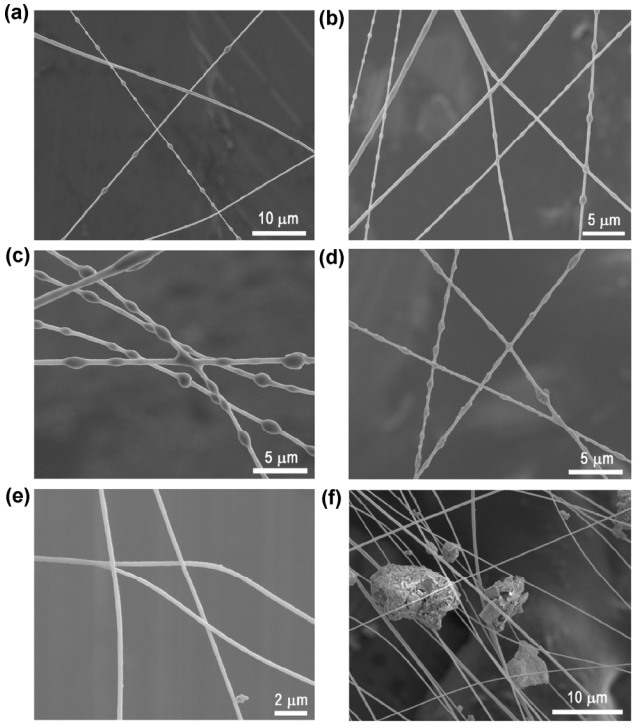

Figure 3 SEM images of $PM_{2.5}$ particles from (a) barbecue smoke, (b) cigarette smoke, (c) incense smoke, (d) wood smoke, (e) car exhaust, and (f) soil dust captured on nanofibers.

of 0.3 μm in exhaust gas was higher than 74.5%, while the proportion of particles with a diameter of 10 μm was only 0.004%, four orders of magnitude lower than the former. The proportions of $PM_{2.5}$ and PM_{10} particles in different sources were compared. As shown in Fig. 2(c), the $PM_{2.5}$ proportions in incense smoke, barbecue smoke, cigarette smoke, wood smoke, and car exhaust were 99.88%, 98.07%, 95.75%, 92.04%, and 99.93%, respectively, clearly indicating high proportions of $PM_{2.5}$ particles. As for the soil dust particles, the proportion of $PM_{2.5}$ particles was 79.28%, which means that the soil dust had the highest proportion of PM_{10} particles, i.e., 20.72%.

SEM and TEM were used to determine the morphologies of these PM particles more accurately. A significant difference in the morphologies of $PM_{2.5}$ and PM_{10} particles was observed. As shown in Figs. 3(a)–3(d), the morphologies of $PM_{2.5}$ particles from smoke on the PI nanofibers were similar. The size distribution of these $PM_{2.5}$ particles was narrow. Almost all combustion smoke, regardless of the type, contained a large amount of oil-like liquid droplets, which can move along the nanofibers and coalesce with each other (see Figs. S9(a)–S9(c) in the ESM). Once the droplets are captured by the nanofibers, they will immediately wrap around the nanofibers owing to surface tension (Fig. S10 in the ESM), forming an axial-symmetric structure, which increases the contact area and adhesion force between the droplets and the nanofibers. The oil-like liquid droplets will gradually become solid particles in ambient conditions after several hours at room temperature (Figs. S9(d) and S9(e) in the ESM). Figure 4 shows the TEM images of the $PM_{2.5}$ particles captured on the Lacey carbon TEM grids, which contain a lot of carbon nanofibers. As shown in Figs. 3(a)–3(d) and 4(a)–4(h), the $PM_{2.5}$ particles from the four different smoke sources can wrap completely around both the PI and carbon nanofibers and form axial-symmetric structures. The contact angles of the smoke particles on both PI nanofibers and carbon nanofibers were small (< 30°, see Table S1 in the ESM), and there was strong adhesion between the smoke particles and the nanofibers.

As for the $PM_{2.5}$ particles from car exhaust and soil dust, the cases are different from those of the smoke sources. The $PM_{2.5}$ particles from exhaust and soil dust are originally in the solid state. Generally, the morphologies of these solid particles will not change when the particles are captured by nanofibers. The morphologies of these solid $PM_{2.5}$ particles were irregular. Unlike the liquid droplets, the solid particles cannot move along the nanofibers and coalesce with

each other. The adhesion between these solid particles and the nanofibers is much weaker than that between smoke particles and nanofibers. As shown in Figs. 3(e) and 3(f), these solid $PM_{2.5}$ particles were attached to the nanofiber only through a small portion of their outer surfaces. The solid particles were mainly captured by the nanofibers through van der Waals forces. As shown in Figs. 3(e), 4(i), and 4(j), there were very few $PM_{2.5}$ particles on the nanofibers from car exhaust. The size and number distribution of the $PM_{2.5}$ particles from soil dust on the nanofibers were random (Figs. 3(f), 4(k), and 4(l)). In addition, they do not have a regular morphology or structure, unlike oil-liquid droplets. Newly arriving particles will attach to both the uncovered parts of the nanofibers and the existing particles. Finally, many dendritic structures will appear with the continuous capture of dust particles (Fig. S11 in the ESM).

As stated above, there are significant differences in the structures, morphologies, and capture mechanisms of $PM_{2.5}$ and PM_{10} particles. The PM_{10} particles from different sources are shown in Fig. 5. As shown in Fig. 5, regardless of the PM source, PM_{10} particles do not have regular morphologies and sizes. According to their morphologies and elemental compositions, these PM_{10} particles are generally classified into the following three types: Soot aggregates, minerals, and fly ashes [37]. Soot aggregates are characterized by their fluffy morphologies, whereas minerals often have elongated and bar morphologies. Fly ashes are mostly round or coated with other fine particles. As shown in Figs. 5(a)–5(d), most of the PM_{10} particles from smoke are soot aggregates, while small portions are fly ashes or mineral particles (Figs. 5(c2), 5(c3), and 5(d4)). As the smoke is produced through the combustion of biomass, a lot of soot aggregates is generated. The soot aggregates have some distinctive characteristics. They are usually formed from ultrafine particles and readily aggregate together before being captured on nanofibers, developing from small groups or chains into larger chains. In addition to the soot aggregates, combustion also produces some fly ashes in PM_{10} particles, especially for the particles from barbecue and wood smoke. Fly ash is composed mainly of non-combustible inorganic material, but also contains some carbon left over from partially combusted wood (Figs. 5(a1)–5(a4), 5(e1)–5(e4), and 5(f1)–5(f4)). PM_{10} particles from car exhaust are only amorphous carbon (see Fig. 7(d)). These amorphous carbon particles have relatively small diameters (Figs. 5(e1)–5(e4)). The morphology of PM_{10} particles from soil dust was slightly more regular than those of smoke PM_{10} particles (Figs. 5(f1)–5(f4)). There were some even larger PM particles with diameters of 10–30 μm (Fig. S8 in the

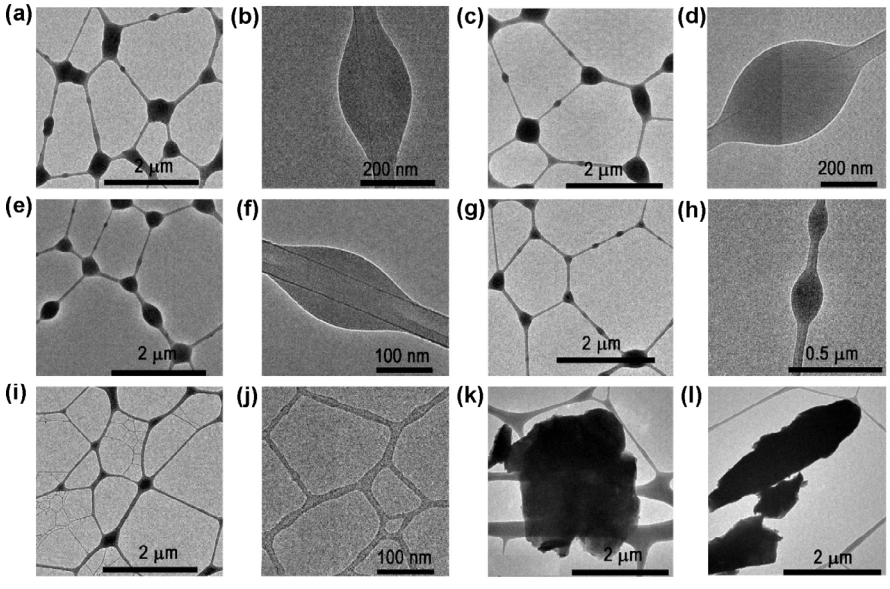

Figure 4 TEM images of $PM_{2.5}$ particles from (a) and (b) barbecue smoke, (c) and (d) cigarette smoke, (e) and (f) incense smoke, (g) and (h) wood smoke, (i) and (j) car exhaust, (k) and (l) soil dust.

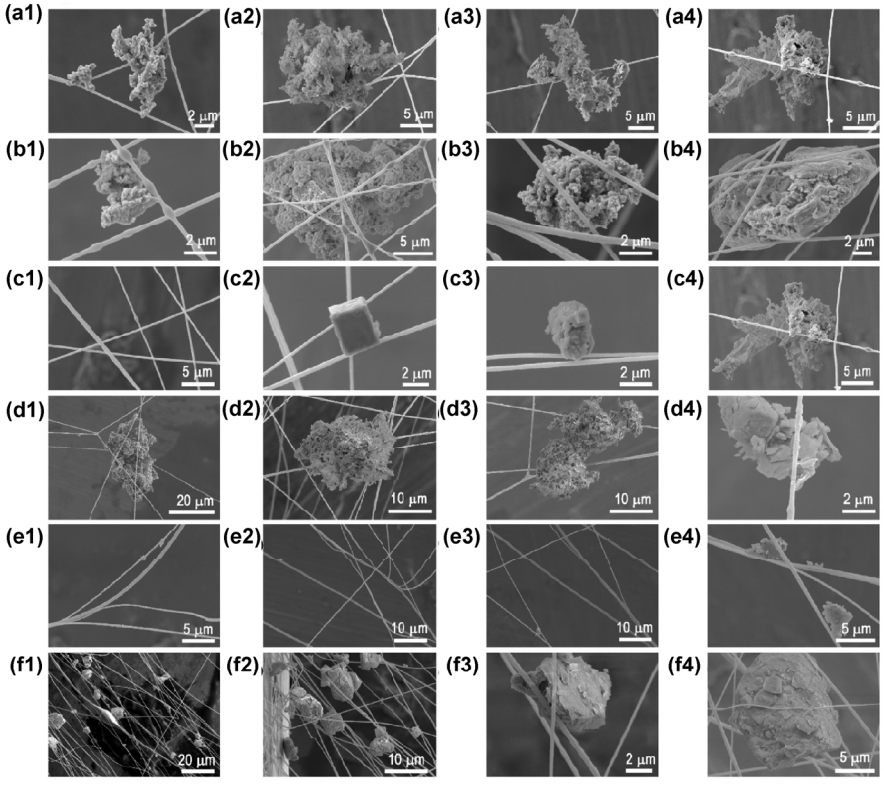

Figure 5 SEM images of PM_{10} particles from (a) barbecue smoke, (b) cigarette smoke, (c) incense smoke, (d) wood smoke, (e) car exhaust, and (f) soil dust captured on nanofibers.

ESM). Most of the dust $PM_{2.5}$ and PM_{10} particles are minerals (Figs. 5(f1)–5(f4)), which is very common in dust particles. It has been reported that feldspar, gypsum, dolomite, calcite, and quartz are the main components in mineral PM particles [37]. EDX analysis showed that they usually consisted of O, Al, and Si, coupled with Na, Ca, Fe, Mg, Br, or other elements (Figs. 7(g) and 7(h)), indicating that there are a lot of inorganic components in these mineral particles.

For the PM particles from smoke, there is a significant difference between the capture mechanisms of $PM_{2.5}$ and PM_{10} particles. Because they are initially liquid droplets, $PM_{2.5}$ particles can change their morphologies to wrap completely around the nanofibers. Then, the liquid droplets gradually become solid particles. Thus, the adhesion between the smoke $PM_{2.5}$ particles and the nanofibers is strong. In comparison, the solid PM_{10} particles are only attached to the nanofibers through part of their outer surfaces and the adhesion between them is weak. In addition, some of them are even captured through direct interception of the nanofiber network (Figs. 5(b2)–5(b4)). As for the PM particles from car exhaust and soil dust, there are no significant differences between the capture mechanisms of $PM_{2.5}$ and PM_{10} particles, as they are all solid particles.

In order to elucidate further the differences among PM particles from different sources, the compositions and surface chemistries of these PM particles were investigated further. We used two methods to characterize these PM particles. First, because of their distinct structural and morphological differences from other types of PM particles, the smoke $PM_{2.5}$ particles were characterized using XPS, which only detects the surface elements (~5 nm in depth). Second, EDX was used to characterize the $PM_{2.5}$ particles from soil dust and car exhaust and the PM_{10} particles from all sources. As shown in Fig. 6(a), for the $PM_{2.5}$ particles from barbecue smoke, the C 1s signal from XPS comprises three major peaks at 284.5, 285.7, and 288.6 eV, corresponding to C–C/C=C, C–H, and C=O bonds. The O 1s peaks support the C 1s peaks and show the presence of C=O at 531.9 eV. A small amount of N is present on the surface of smoke particles, as indicated by the peak at 400.1 eV, representing the $–NH_2$ functional group.

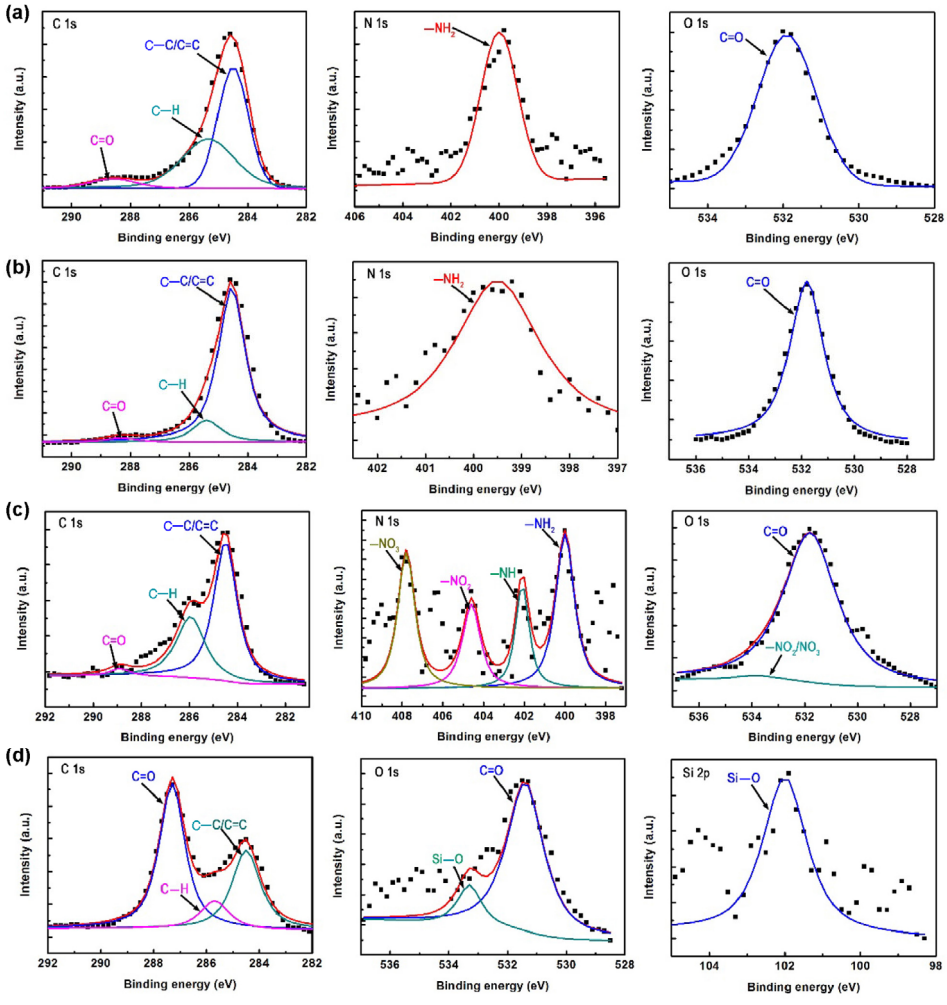

Figure 6 XPS characterization of $PM_{2.5}$ particles from (a) barbecue smoke, (b) cigarette smoke, (c) incense smoke, and (d) wood smoke captured on nanofibers.

The overall results show that C, O, H, and N are the four elements present on the $PM_{2.5}$ particles from barbecue smoke. The $PM_{2.5}$ particles from cigarette smoke showed very similar XPS characteristics to those of barbecue $PM_{2.5}$ particles, showing only C 1s, O 1s, and N 1s peaks (Fig. 6(b)). The XPS results for $PM_{2.5}$ particles from incense smoke were similar, also showing that C, O, N, and H are the four elements present (Fig. 6(c)). However, the N 1s peaks are different. As shown in Fig. 6(c), the N 1s signal comprises four major peaks at 400, 402.1, 404.6, and 407.8 eV, corresponding to $–NH_2$, –NH, $–NO_2$, and $–NO_3$ functional groups, respectively. The XPS results for the $PM_{2.5}$ particles from wood smoke were slightly different. The C 1s signal comprises three major peaks at 284.5, 285.7, and 287.3 eV, corresponding to C–C/C=C, C–H, and C=O bonds. Moreover, a small amount of Si is present on the surface of smoke particles, as indicated by the peak at 100.8 eV in the Si 2p peak, representing Si–O bonds. The O 1s peaks support the C 1s and Si 2p peaks and show the presence of C=O at 531.4 eV and Si–O at 533.3 eV. The $PM_{2.5}$ particles from barbecue smoke also have four elements, i.e., C, O, N, and H. From the above analysis, we can infer that the $PM_{2.5}$ particles from different smoke sources have similar components, mainly C, H, O, and N, clearly showing that they are organic aerosols.

The effect of temperature on the morphologies of $PM_{2.5}$ particles from smoke was also investigated. Here, we take the PM particles from incense smoke as an example. It has been reported that incense smoke contains many components, such as CO, CO_2, NO_2,

and also volatile organic compounds such as benzene, toluene, xylenes, aldehydes, polycyclic aromatic hydrocarbons, etc. [41]. Many of these components are not stable and will decompose at high temperatures. Thus, the structures and morphologies of these particles will change as the temperature increases owing to the decomposition of many organic components. It was found that, as the temperature increased, the diameter of the incense smoke particles gradually decreased (Figs. S12–S16 in the ESM).

The chemical compositions of the PM_{10} particles from the above six sources were analyzed using EDX. It was found that there were no significant differences between the $PM_{2.5}$ particles from soil dust and car exhaust and the PM_{10} particles from the same two sources. Unlike the XPS results for the $PM_{2.5}$ particles from smoke sources, those of the PM_{10} particles showed significant differences. For instance, the $PM_{2.5}$ particles from barbecue smoke contain only C, O, H, and N (Fig. 6(a)), but the PM_{10} particles contain C, O, Na, Br, Si, and Ca (Fig. 7(a)), indicating that the PM_{10} particles contain many inorganic components. As mentioned above, the PM_{10} particles from smoke contain a lot of soot aggregates, fly ashes, and some minerals; thus, their compositions are more complicated than those of the organic particles. The PM_{10} particles from cigarette smoke, which contain C, O, Fe, Na, Al, P, Cl, and K (Fig. 7(b)), showed a similar characteristic. Compared to the PM_{10} particles from barbecue (Fig. 7(a)), cigarette (Fig. 7(b)), and incense smoke (Fig. 7(c)), the PM_{10} particles from wood smoke were more complicated (Figs. 7(e) and 7(f)). Different PM_{10}

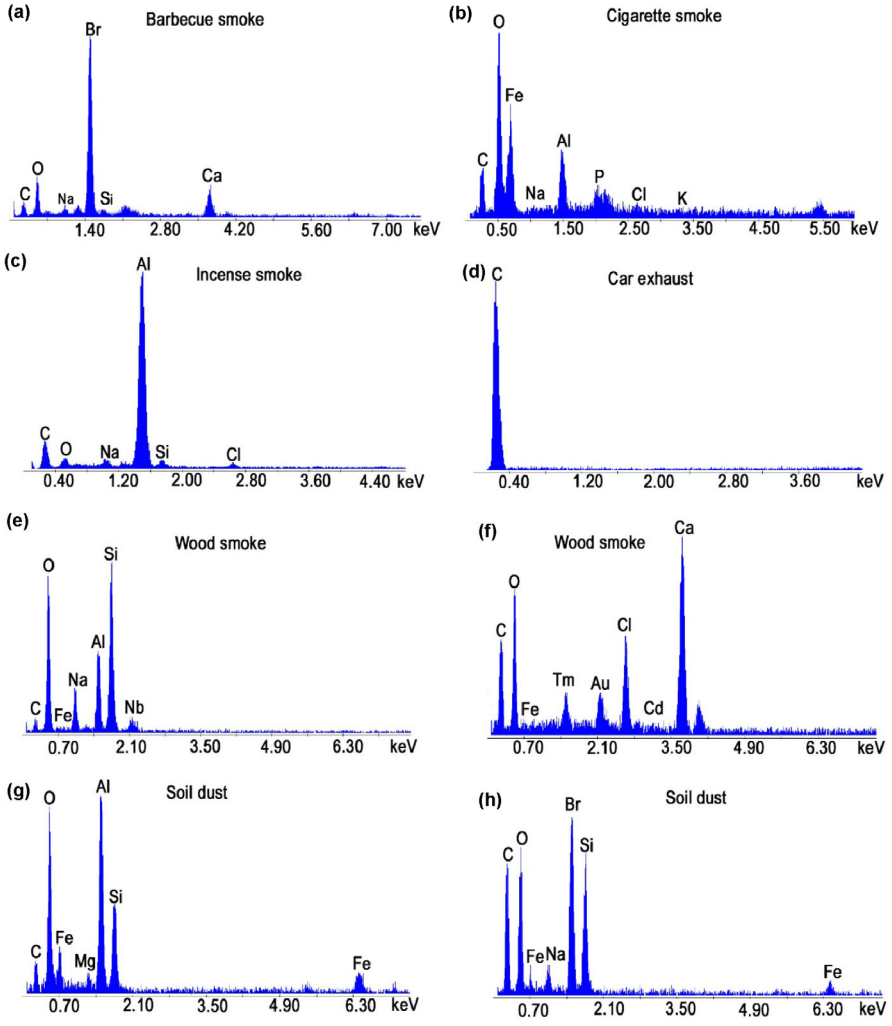

Figure 7 EDX characterization of PM_{10} particles from (a) barbecue smoke, (b) cigarette smoke, (c) incense smoke, (d) car exhaust, (e) and (f) wood smoke, and (g) and (h) soil dust captured on nanofibers.

particles from wood smoke contained different elements. The PM_{10} particles from soil dust showed a similar characteristic, indicating that they also have a complicated composition (Figs. 7(g) and 7(h)). The only unique sample was the PM_{10} particles from car exhaust, which contained only C (Fig. 7(d)), indicating that they are mainly amorphous carbon from the incomplete combustion of gasoline.

In summary, we have characterized PM_{10} and $PM_{2.5}$ particles from six different sources and compared their morphologies, concentration distributions, compositions, and capture mechanisms. Different types of PM particles exhibit different characteristics. For almost all types of PM particles, the PM concentration, with certain sizes, decreases continuously as the size increases. Most of the PM particles from smoke are $PM_{2.5}$ particles with narrow size distributions. There are very few PM particles in car exhaust. The proportion of PM_{10} particles in soil dust is much higher than those in other sources. The $PM_{2.5}$ particles from smoke exhibit an axial-symmetrical structure on PI nanofibers with a narrow diameter distribution. In comparison, regardless of the PM source, PM_{10} particles are stochastic, without a regular morphology or structure. According to their morphologies and elemental compositions, these PM_{10} particles are generally classified into the following three types: Soot aggregates, minerals, and fly ashes. Most of the PM_{10} particles from smoke are soot aggregates, while small portions are fly ashes and mineral particles. PM particles from car exhaust are only amorphous carbon. Most of the dust PM particles are minerals. For the PM particles from smoke, there is a significant difference between the capture mechanisms of $PM_{2.5}$ and PM_{10} particles. The $PM_{2.5}$ particles from smoke can change their morphologies to wrap completely around the nanofibers, and thus, the adhesion between them and the nanofibers is strong. In comparison, the solid PM_{10} particles attach to the nanofibers through only part of their outer surfaces and exhibit weak adhesion with the nanofibers. XPS showed that the $PM_{2.5}$ particles from different smoke sources have similar components, mainly consisting of C, H, O, and N. The effect of temperature on the morphologies of $PM_{2.5}$ particles from smoke was also investigated and it was found that they will decompose as the temperature increases. The compositions of the PM_{10} particles were complicated, and these particles consisted mainly of inorganic components.

Acknowledgements

We thank Dr. Yuanqing Li for fruitful discussions.

Electronic Supplementary Material: Supplementary material (supplementary figures) is available in the online version of this article at https://doi.org/10.1007/s12274-017-1724-y.

References

[1] Fang, M.; Chan, C. K.; Yao, X. H. Managing air quality in a rapidly developing nation: China. *Atmos. Environ.* **2009**, *43*, 79–86.

[2] Seinfeld, J. H. Urban air pollution: State of the science. *Science* **1989**, *243*, 745–752.

[3] Zhang, R.; Jing, J.; Tao, J.; Hsu, S. C.; Wang, G.; Cao, J.; Lee, C. S. L.; Zhu, L.; Chen, Z.; Zhao, Y. et al. Chemical characterization and source apportionment of $PM_{2.5}$ in Beijing: Seasonal perspective. *Atmos. Chem. Phys.* **2013**, *13*, 7053–7074.

[4] Maricq, M. M. Chemical characterization of particulate emissions from diesel engines: A review. *J. Aerosol Sci.* **2007**, *38*, 1079–1118.

[5] Makkonen, U.; Hellén, H.; Anttila, P.; Ferm, M. Size distribution and chemical composition of airborne particles in south-eastern Finland during different seasons and wildfire episodes in 2006. *Sci. Total Environ.* **2010**, *408*, 644–651.

[6] Betha, R.; Behera, S. N.; Balasubramanian, R. 2013 Southeast Asian smoke haze: Fractionation of particulate-bound elements and associated health risk. *Environ. Sci. Technol.* **2014**, *48*, 4327–4335.

[7] Wu, S. W.; Deng, F. R.; Wei, H. Y.; Huang, J.; Wang, X.; Hao, Y.; Zheng, C. J.; Qin, Y.; Lv, H. B.; Shima, M. et al. Association of cardiopulmonary health effects with source-appointed ambient fine particulate in Beijing, China: A combined analysis from the healthy volunteer natural relocation (HVNR) study. *Environ. Sci. Technol.* **2014**, *48*, 3438–3448.

[8] Brook, R. D.; Rajagopalan, S.; Pope III, C. A.; Brook, J. R.; Bhatnagar, A.; Diez-Roux, A. V.; Holguin, F.; Hong, Y. L.; Luepker, R. V.; Mittleman, M. A. et al. Particulate matter air pollution and cardiovascular disease: An update to the

scientific statement from the American Heart Association. *Circulation* **2010**, *121*, 2331–2378.

[9] Anenberg, S. C.; Horowitz, L. W.; Tong, D. Q.; West, J. J. An estimate of the global burden of anthropogenic ozone and fine particulate matter on premature human mortality using atmospheric modeling. *Environ. Health Perspect.* **2010**, *118*, 1189–1195.

[10] Timonen, K. L.; Vanninen, E.; De Hartog, J.; Ibald-Mulli, A.; Brunekreef, B.; Gold, D. R.; Heinrich, J.; Hoek, G.; Lanki, T.; Peters, A. et al. Effects of ultrafine and fine particulate and gaseous air pollution on cardiac autonomic control in subjects with coronary artery disease: The ULTRA study. *J. Expo. Sci. Environ. Epidemiol.* **2006**, *16*, 332–341.

[11] Zhao, S. H.; Chen, L. Q.; Li, Y. L.; Xing, Z. Y.; Du, K. Summertime spatial variations in atmospheric particulate matter and its chemical components in different functional areas of Xiamen, China. *Atmosphere* **2015**, *6*, 234–254.

[12] Hoek, G.; Krishnan, R. M.; Beelen, R.; Peters, A.; Ostro, B.; Brunekreef, B.; Kaufman, J. D. Long-term air pollution exposure and cardio-respiratory mortality: A review. *Environ. Health* **2013**, *12*, 43.

[13] Zhang, Y. Y.; Yuan, S.; Feng, X.; Li, H. W.; Zhou, J. W.; Wang, B. Preparation of nanofibrous metal–organic framework filters for efficient air pollution control. *J. Am. Chem. Soc.* **2016**, *138*, 5785–5788.

[14] Zhang, R. F.; Liu, C.; Hsu, P. C.; Zhang, C. F.; Liu, N.; Zhang, J. S.; Lee, H. R.; Lu, Y. Y.; Qiu, Y. C.; Chu, S. et al. Nanofiber air filters with high-temperature stability for efficient $PM_{2.5}$ removal from the pollution sources. *Nano Lett.* **2016**, *16*, 3642–3649.

[15] Xu, J. W.; Liu, C.; Hsu, P. C.; Liu, K.; Zhang, R. F.; Liu, Y. Y.; Cui, Y. Roll-to-roll transfer of electrospun nanofiber film for high-efficiency transparent air filter. *Nano Lett.* **2016**, *16*, 1270–1275.

[16] Wang, S.; Zhao, X. L.; Yin, X.; Yu, J. Y.; Ding, B. Electret polyvinylidene fluoride nanofibers hybridized by polytetrafluoroethylene nanoparticles for high-efficiency air filtration. *ACS Appl. Mater. Interfaces* **2016**, *8*, 23985–23994.

[17] Liu, C.; Hsu, P. C.; Lee, H. W.; Ye, M.; Zheng, G. Y.; Liu, N.; Li, W. Y.; Cui, Y. Transparent air filter for high-efficiency $PM_{2.5}$ capture. *Nat. Commun.* **2015**, *6*, 6205.

[18] Gong, G. M.; Zhou, C.; Wu, J. T.; Jin, X.; Jiang, L. Nanofibrous adhesion: The twin of gecko adhesion. *ACS Nano* **2015**, *9*, 3721–3727.

[19] Li, P.; Zong, Y. C.; Zhang, Y. Y.; Yang, M. M.; Zhang, R. F.; Li, S. Q.; Wei, F. *In situ* fabrication of depth-type hierarchical CNT/quartz fiber filters for high efficiency filtration of sub-micron aerosols and high water repellency. *Nanoscale* **2013**, *5*, 3367–3372.

[20] Han, C. B.; Jiang, T.; Zhang, C.; Li, X. H.; Zhang, C. Y.; Cao, X.; Wang, Z. L. Removal of particulate matter emissions from a vehicle using a self-powered triboelectric filter. *ACS Nano* **2015**, *9*, 12552–12561.

[21] Wang, C. Y.; Wu, S. Y.; Jian, M. Q.; Xie, J. R.; Xu, L. P.; Yang, X. D.; Zheng, Q. S.; Zhang, Y. Y. Silk nanofibers as high efficient and lightweight air filter. *Nano Res.* **2016**, *9*, 2590–2597.

[22] Hildemann, L. M.; Rogge, W. F.; Cass, G. R.; Mazurek, M. A.; Simoneit, B. R. T. Contribution of primary aerosol emissions from vegetation-derived sources to fine particle concentrations in Los Angeles. *J. Geophys. Res. Atmos.* **1996**, *101*, 19541–19549.

[23] Xing, J.; Pleim, J.; Mathur, R.; Pouliot, G.; Hogrefe, C.; Gan, C. M.; Wei, C. Historical gaseous and primary aerosol emissions in the United States from 1990 to 2010. *Atmos. Chem. Phys.* **2013**, *13*, 7531–7549.

[24] Limbeck, A.; Kulmala, M.; Puxbaum, H. Secondary organic aerosol formation in the atmosphere via heterogeneous reaction of gaseous isoprene on acidic particles. *Geophys. Res. Lett.* **2003**, *30*, DOI: 10.1029/2003GL017738.

[25] Schuetzle, D.; Cronn, D.; Crittenden, A. L.; Charlson, R. J. Molecular composition of secondary aerosol and its possible origin. *Environ. Sci. Tech.* **1975**, *9*, 838–845.

[26] Huang, R. J.; Zhang, Y. L.; Bozzetti, C.; Ho, K. F.; Cao, J. J.; Han, Y. M.; Daellenbach, K. R.; Slowik, J. G.; Platt, S. M.; Canonaco, F. et al. High secondary aerosol contribution to particulate pollution during haze events in China. *Nature* **2014**, *514*, 218–222.

[27] Wal, R. L. V.; Bryg, V. M.; Hays, M. D. XPS analysis of combustion aerosols for chemical composition, surface chemistry, and carbon chemical state. *Anal. Chem.* **2011**, *83*, 1924–1930.

[28] Jang, M.; Czoschke, N. M.; Lee, S.; Kamens, R. M. Heterogeneous atmospheric aerosol production by acid-catalyzed particle-phase reactions. *Science* **2002**, *298*, 814–817.

[29] Li, W. J.; Shao, L. Y.; Zhang, D. Z.; Ro, C. U.; Hu, M.; Bi, X. H.; Geng, H.; Matsuki, A.; Niu, H. Y.; Chen, J. M. A review of single aerosol particle studies in the atmosphere of East Asia: Morphology, mixing state, source, and heterogeneous reactions. *J. Cleaner Prod.* **2015**, *112*, 1330–1349.

[30] Wang, J.; Hu, Z. M.; Chen, Y. Y.; Chen, Z. L.; Xu, S. Y. Contamination characteristics and possible sources of PM_{10} and $PM_{2.5}$ in different functional areas of Shanghai, China. *Atmos. Environ.* **2013**, *68*, 221–229.

[31] Pope III, C. A.; Dockery, D. W.; Spengler, J. D.; Raizenne, M. E. Respiratory health and PM_{10} pollution: A daily time series analysis. *Am. Rev. Respir. Dis.* **1991**, *144*, 668–674.

[32] Pope III, C. A.; Schwartz, J.; Ransom, M. R. Daily mortality and PM_{10} pollution in Utah Valley. *Arch. Environ. Health* **1992**, *47*, 211–217.

[33] Pope III, C. A.; Dockery, D. W. Acute health effects of PM_{10} pollution on symptomatic and asymptomatic children. *Am. Rev. Respir. Dis.* **1992**, *145*, 1123–1128.

[34] Ostro, B. D.; Hurley, S.; Lipsett, M. J. Air pollution and daily mortality in the Coachella Valley, California: A study of PM_{10} dominated by coarse particles. *Environ. Res.* **1999**, *81*, 231–238.

[35] Yue, W. S.; Li, X. L.; Liu, J. F.; Li, Y.; Yu, X. H.; Deng, B.; Wan, T. M.; Zhang, G. L.; Huang, Y. Y.; He, W. et al. Characterization of $PM_{2.5}$ in the ambient air of Shanghai city by analyzing individual particles. *Sci. Total Environ.* **2006**, *368*, 916–925.

[36] Labrada-Delgado, G.; Aragon-Pina, A.; Campos-Ramos, A.; Castro-Romero, T.; Amador-Munoz, O.; Villalobos-Pietrini, R. Chemical and morphological characterization of $PM_{2.5}$ collected during MILAGRO campaign using scanning electron microscopy. *Atmos. Pollut. Res.* **2012**, *3*, 289–300.

[37] Feng, X. D.; Dang, Z.; Huang, W. L.; Shao, L. Y.; Li, W. J. Microscopic morphology and size distribution of particles in $PM_{2.5}$ of Guangzhou City. *J. Atmos. Chem.* **2009**, *64*, 37–51.

[38] Longhin, E.; Holme, J. A.; Gutzkow, K. B.; Arlt, V. M.; Kucab, J. E.; Camatini, M.; Gualtieri, M. Cell cycle alterations induced by urban $PM_{2.5}$ in bronchial epithelial cells: Characterization of the process and possible mechanisms involved. *Part. Fibre Toxicol.* **2013**, *10*, 63.

[39] Deng, X. B.; Zhang, F.; Rui, W.; Long, F.; Wang, L. J.; Feng, Z. H.; Chen, D. L.; Ding, W. J. $PM_{2.5}$-induced oxidative stress triggers autophagy in human lung epithelial A549 cells. *Toxicol. Vitro* **2013**, *27*, 1762–1770.

[40] Hueglin, C.; Gehrig, R.; Baltensperger, U.; Gysel, M.; Monn, C.; Vonmont, H. Chemical characterisation of $PM_{2.5}$, PM_{10} and coarse particles at urban, near-city and rural sites in Switzerland. *Atmos. Environ.* **2005**, *39*, 637–651.

[41] Lin, T. C.; Krishnaswamy, G.; Chi, D. S. Incense smoke: clinical, structural and molecular effects on airway disease. *Clin. Mol. Allergy* **2008**, *6*, 3.